J. Vis. Commun. Image R. 36 (2016) 1–10

Contents lists available at ScienceDirect

J. Vis. Commun. Image R.

journal homepage: www.elsevier.com/locate/jvci

A neutrosophic filter for high-density Salt and Pepper noise based on pixel-wise adaptive smoothing parameter ☆

Xianying Qi [a,b], Boqiang Liu [a,*], Jianwei Xu [c]

[a] School of Control Science and Engineering, Shandong University, Jinan, Shandong 250010, China
[b] Department of Radiology, Taishan Medical University, Taian, Shandong 271000, China
[c] Medical Imaging Department, Taian Tumor Prevention and Treatment Hospital, Taian, Shandong 271000, China

ARTICLE INFO

Article history:
Received 2 January 2015
Accepted 6 January 2016
Available online 11 January 2016

Keywords:
Image denoising
Salt and Pepper noise
Adaptive neutrosophic weight function
Pixel-wise adaptive smoothing parameter
Indicator of image contents
Similarity measurement
Neutrosophic Set
Indeterminacy

ABSTRACT

Image indeterminacy has been neglected in most traditional filtering algorithms. This paper proposes a pixel-wise adaptive neutrosophic filter based on neutrosophic indeterminacy feature to remove high-level Salt-and-Pepper noise. In the proposed algorithm, the indeterminacy of a pixel is quantified by a Neutrosophic Set and innovatively exploited as an efficient characteristic of measuring the similarity of pixels. In order to adjust the smoothing parameter of the weight function pixel-wise adaptively, the uncertainty of a pixel is utilized as an indicator of image contents. Extensive experiments on numerous images demonstrate that with a 3×3 window, our method outperforms many existing denoising methods in terms of noise suppression and detail preservation.

1. Introduction

Noise is an unwanted signal that corrupts the original image in various processes such as image acquisition, transmission and storage. The aim of image denoising is to remove noise while retaining useful details as much as possible. One of the most destructive noises is Salt-and-Pepper noise (SPN) that replaces the original pixels with the maximum or minimum gray level of the image. Quality of the original image is deteriorated significantly, so it is imperative to eliminate noise before subsequent image processing, such as object recognition and image segmentation.

Numerous methods have been proposed to remove SPN. The most popular nonlinear filter is the median filter (MF) [1], but strong, undesired contouring effect is produced by MF. It performs well only in low-density noise and under high-density (>70%) environment [2], a larger window size can improve the performance of noise removal; however, it makes a looser correlation between the median value and the corrupted pixel, which leads to the blurring of image details [2,3]. Furthermore, the most appropriate window size varies with the density of noise, so it is rather difficult to choose the optimal one. To automatically adjust the window size, an adaptive median filter (AMF) has been put forward in [4,5], but at high noise density (HND), the biggest template size has reached 39×39, and the computation is exceedingly heavy. Another drawback of MF is that it executes identically on all pixels in the image, yet an ideal filter should be applied only to noisy pixels while leaving noise-free pixels intact. Hence, a switching median filter (SMF) [6] was introduced to avoid the injuring of uncontaminated pixels. In SMF, noisy pixels are firstly identified by certain strategies and then removed by specialized regularizations. There are some well-known methods with the switching scheme, such as decision-based algorithm (DBA) [7], switching-based adaptive weighted median (SAWM) [8], modified decision based unsymmetrical trimmed median filter (MDBUTM) [9], fuzzy-based decision algorithm (FBDA) [10], and decision-based trimmed median filter (DBTMF) [11]. In DBA, if a pixel has a gray value of 0 or 255 in 8-bit image, it is considered to be a noise candidate. In noise reduction stage, the noise candidate is replaced by the median value as long as at least one noise-free pixel exists in the 3×3 window, otherwise it will be replaced by its neighborhood pixels. Nevertheless, this kind of repetitive replacement results in annoying artifacts in HND. To overcome this problem, when all pixels are contaminated, MDBUTMF substitutes the mean value of all noisy elements in the filtering template for the center pixel, which generates artificial spots in the restored image. It is clear that the drawback common to DBA and MDBUTMF is that they all ignore the correlation between pixels. In FBDA, the

☆ This paper has been recommended for acceptance by Yehoshua Zeevi.

* Corresponding author.
E-mail addresses: xyqi@tsmc.edu.cn (X. Qi), qxy9228@163.com (B. Liu).

http://dx.doi.org/10.1016/j.jvcir.2016.01.005
1047-3203/

maximum and minimum of window gray value are regarded as noisy points, and the pixels similar to these polluted ones are all eliminated by a fuzzy mechanism. Then the median of the remaining elements is exploited to refresh the center pixel. The strategy of DBTMF is similar to that of FBDA and the only difference between them is that the median value is computed after eliminating pixels with the value of 0 or 255. The major disadvantage of these extreme-compression methods is that only the high reliability of the median is considered while the local information of pixels has been neglected. Consequently, details and edges cannot be recovered satisfactorily. In order to overcome this shortcoming, the theory of image inpainting has been introduced to preserve edges. In [12,13], a three-stage filter (TSF) and an adaptive iterative convolutions filter (ACIF) have been proposed, respectively. They can not only suppress noise, but also preserve edge information efficiently. However, on account of iterative inpainting, the phenomenon of undue blurring or over-smoothing is obvious in the restored image at HND. In non-local means (NLM) [14,15] filter, a weighting scheme is applied, where the weight is determined by the similarity of local patches. NLM is powerful against Gaussian noise, but performs poor in SPN. Besides, in the weight functions of most NLM filters, the value of the smoothing parameter h is usually set manually. Methods for adaptive h have been studied [15,16], but on account of having not taken image contents into consideration, most algorithms still use a globally constant value of h.

Due to the complexity of noise sources and the imperfection of certain definitions, such factors as ambiguity, vagueness and imprecision are widespread in image processing. Nevertheless, algorithms above-mentioned have not taken them into account. Unlike conventional algorithms, in [17], the indeterminacy information is introduced to image denoising and a Neutrosophic entropy filter (NEF) has been presented. In NEF, the contaminated image is transformed into Neutrosophic Set (NS) domain at first, then an iterative γ-median filtering is applied to reduce the indetermination degree evaluated by neutrosophic entropy. It can remove different kinds of noises effectively, but the iterative operation of γ-median generates undue blurring of images. At present, Neutrosophy has been used not only in image denoising but also in image segmentation [18,19]. Consequently, how to further maximize the potential of indeterminacy in image restoration is a meaningful task.

In this paper, by exploiting the indeterminacy information based on NS, a new powerful neutrosophic filter is presented for the reduction of high density SPN. On one hand, the uncertainty of a pixel is regarded as a feature of measuring pixel similarity; on the other hand, by using the indeterminate information to distinguish the regional type to which a pixel belongs, a pixel-wise adaptive smoothing function is put forward to minimize the negative influence resulting from a globally fixed h. Experimental results on a series of images have demonstrated that the proposed adaptive neutrosophic weighted filter (ANWF) outperforms the counterparts in terms of visual quality and objective performance.

The outline of the paper is organized as follows. NS and the quantification of uncertainty are briefly introduced in Section 2. Section 3 describes ANWF in detail. Results of the proposed algorithm are described and discussed in Section 4. Section 5 concludes the paper.

2. Quantification of indeterminacy

2.1. Neutrosophic Set

Proposed by Florentine Smarandache, Neutrosophy is the foundation of neutrosophic logic, neutrosophic statistics, Neutrosophic Set and neutrosophic probability [20,21]. In neutrosophic logic, ⟨A⟩ is a theory, entity or event, and ⟨Anti-A⟩ is the opposite of ⟨A⟩. A new concept ⟨Neut-A⟩ is introduced to express the case of neither ⟨A⟩ nor ⟨Anti-A⟩ and used to describe the indeterminacy of an event [21]. For example, if ⟨A⟩ = black, then ⟨Anti-A⟩ = white, ⟨Neut-A⟩ = red, green, purple, cyan, blue, yellow, etc. (any color except white and black). In the contaminated image, sometimes it is difficult to distinguish whether a pixel is noisy or noise-free due to the existing of textures or boundaries. In this paper, we denote the background of image as ⟨A⟩, the edge or texture as ⟨Neut-A⟩, and noise as ⟨Anti-A⟩. Three neutrosophic components denoted by T, I and F are applied to estimate the degrees of truth, indeterminacy and false, respectively. Let T, I and F be non-standard or standard real subsets of $]-0,1+[$ with $\sup T = t\_\sup$, $\inf T = t\_\inf$, $\sup I = i\_\sup$, $\inf I = i\_\inf$, $\sup F = f\_\sup$, $\inf F = f\_\inf$, and $n\_\sup = t\_\sup + i\_\sup + f\_\sup$,$n\_\inf = t\_\inf + i\_\inf + f\_\inf$ [29]. Where $x\_\sup$ and $x\_\inf$ are the superior and inferior limits of subset x. There are no restriction on $n\_\sup$ *and* $n\_\inf$, so $^{-}0 \leqslant n\_\sup \leqslant 3^{+}$ and $^{-}0 \leqslant n\_\inf \leqslant 3^{+}$. T, I and F can be any real sub-unitary subsets and are not necessarily intervals. Besides, the three sets may overlap or be converted from one to the other [30]. An element A (t, i, f) belongs to the set in the following way: it is t true ($t \in T$), i indeterminate ($i \in I$), and f false ($f \in F$). In Neutrosophy, if an event ⟨A⟩ is t % true, it does not necessarily mean it is $(1-t)$ % false, but can be f % false and i % indeterminate simultaneously. However, in traditional logic, if an event ⟨A⟩ is t % true, it must be $(1-t)$ % false.

2.2. Neutrosophic image

In neutrosophic domain, a neutrosophic image P_{NS} is represented by three sets I, T and F [19], and a neutrosophic pixel is denoted as $P(t,i,f)$. The expression of neutrosophic pixel signifies the point is t % true (background), i % indeterminate (texture or edge) and f % false (noise), where i varies in I, t varies in T, and f varies in F, respectively. A pixel $P(i,j)$ in traditional image can be transformed into neutrosophic domain in the following way: $P_{NS}(i,j) = \{T(i,j), I(i,j), F(i,j)\}$. In order to make full use of the uncertain information to restore the corrupted image, an efficient estimation of I is critical. It is well known that the median value has stronger immunity to SPN, so it can be used to construct the function of I. Besides, the maximum absolute luminance difference defined as Eqs. (1) and (2) can reflect the distinction between the center pixel and its neighboring pixels, hence it can be utilized to evaluate the degree of current pixel being noise-free.

$$Dif(i,j) = \max\{dif(i+k,j+l)\}, \tag{1}$$

$$dif(i+k,j+l) = |p(i+k,j+l) - p(i,j)| \quad with\ (i+k,j+l) \neq (i,j), \tag{2}$$

Motivated by Ref. [17], $I(i,j), T(i,j)$ and $F(i,j)$ are formulated as

$$I(i,j) = \frac{\delta(i,j) - \delta_{\min}}{\delta_{\max} - \delta_{\min}}, \tag{3}$$

$$\delta(i,j) = |P(i,j) - m(i,j)|, \tag{4}$$

$$m(i,j) = median \begin{bmatrix} p(i-1,j-1) & p(i-1,j) & p(i-1,j+1) \\ p(i,j-1) & p(i,j) & p(i,j+1) \\ p(i+1,j-1) & p(i+1,j) & p(i+1,j+1) \end{bmatrix}, \tag{5}$$

$$T(i,j) = \frac{Dif_{\max} - Dif(i,j)}{Dif_{\max} - Dif_{\min}}, \tag{6}$$

$$F(i,j) = 1 - T(i,j). \tag{7}$$

where $m(i,j)$ is the local median value of the $w \times w$ window ($w = 2n+1$ $(n \geqslant 1)$) centered at (i,j), and in a 3×3 window, it

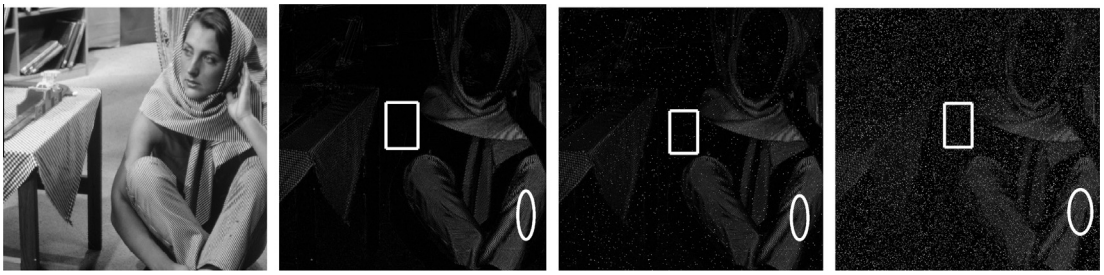

Fig. 1. Images of indeterminacy in NS. (a) Original image. (b) Indeterminacy image of original Babala. (c) Indeterminacy of noisy image (σ = 1%). (d) Indeterminacy of noisy image (σ = 10%).

Fig. 2. Standard images used for searching optimal *K*. (a) Lena. (b) Peppers. (c) Tree-hill. (d) Cat. (e) Buildings.

can be presented as Eq. (5). $\delta(i,j)$ denotes the absolute difference between $P(i,j)$ and $m(i,j)$ and $Dif(i,j)$ is the maximum absolute luminance difference in working window. For an image with a size of $M \times N$, $\delta_{\max}$, $\delta_{\min}$, $Dif_{\max}$ and $Dif_{\min}$ are described as

$$\delta_{\max} = \max\{\delta(s,t)\},\ \ \delta_{\min} = \min\{\delta(s,t)\}(s \in M, t \in N). \tag{8}$$

$$Dif_{\max} = \max\{Dif(s,t)\},\ \ Dif_{\min} = \min\{Dif(s,t)\}(s \in M, t \in N). \tag{9}$$

From above formulas, we can conclude that if $\delta(i,j)$ is larger, $P(i,j)$ will has a lower reliability, and vice versa. So normalized by the factor of $\delta_{\max} - \delta_{\min}$, $\delta(i,j)$ can estimate the indeterminacy degree of $P(i,j)$. Likewise, a lager $Dif(i,j)$ signifies $P(i,j)$ has a looser relation with surrounding pixels; hence, after normalized by $Dif_{\max} - Dif_{\min}$, it has the capability to calculate the truth degree of $P(i,j)$ being signal pixel. In this paper, the introductions of $T(i,j)$ and $F(i,j)$ are just to illustrate the process of transforming an image from traditional field to NS domain, but they have not been used in noise reduction.

2.3. Properties of neutrosophic indeterminacy

From Eqs. (3–5), we can deduce that if $P(i,j)$ has a similar value with the median of a squared window, its $I(i,j)$ will be lower; therefore pixels in smooth area will have a lower indeterminacy. While in edge zones, due to the stronger gray fluctuation, pixels will have a slightly larger indeterminacy. Nonetheless, compared with the vibration intensity of SPN, the gray variation on edge is comparatively moderate. This is because there are certain correlations between pixels in edge zones and their intensity variation are relatively continuous. Yet SPN has no relevancy with their neighborhoods and they only take the maximum or the minimum value

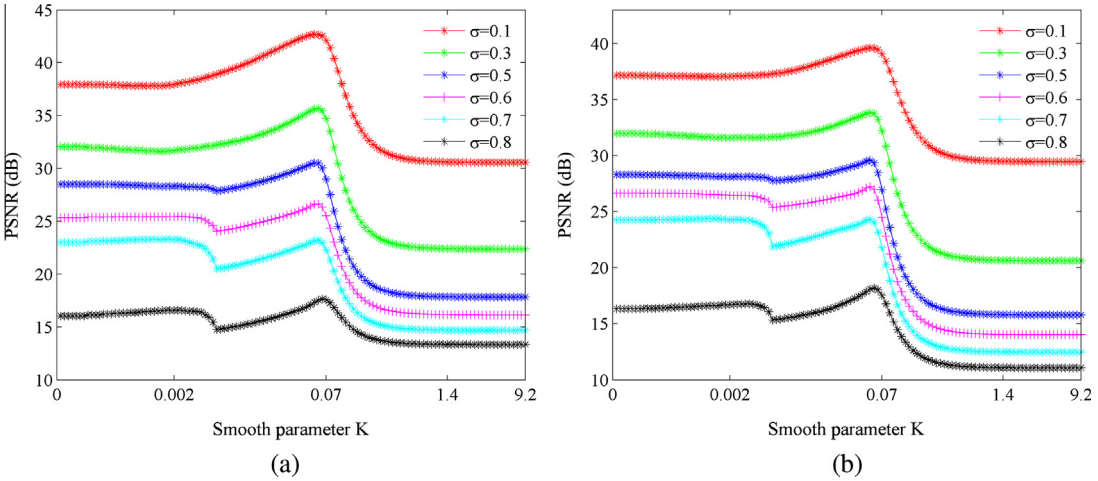

Fig. 3. The relation between *K* and the PSNR at different noise levels. (a) Lena image. (b) Cat image.

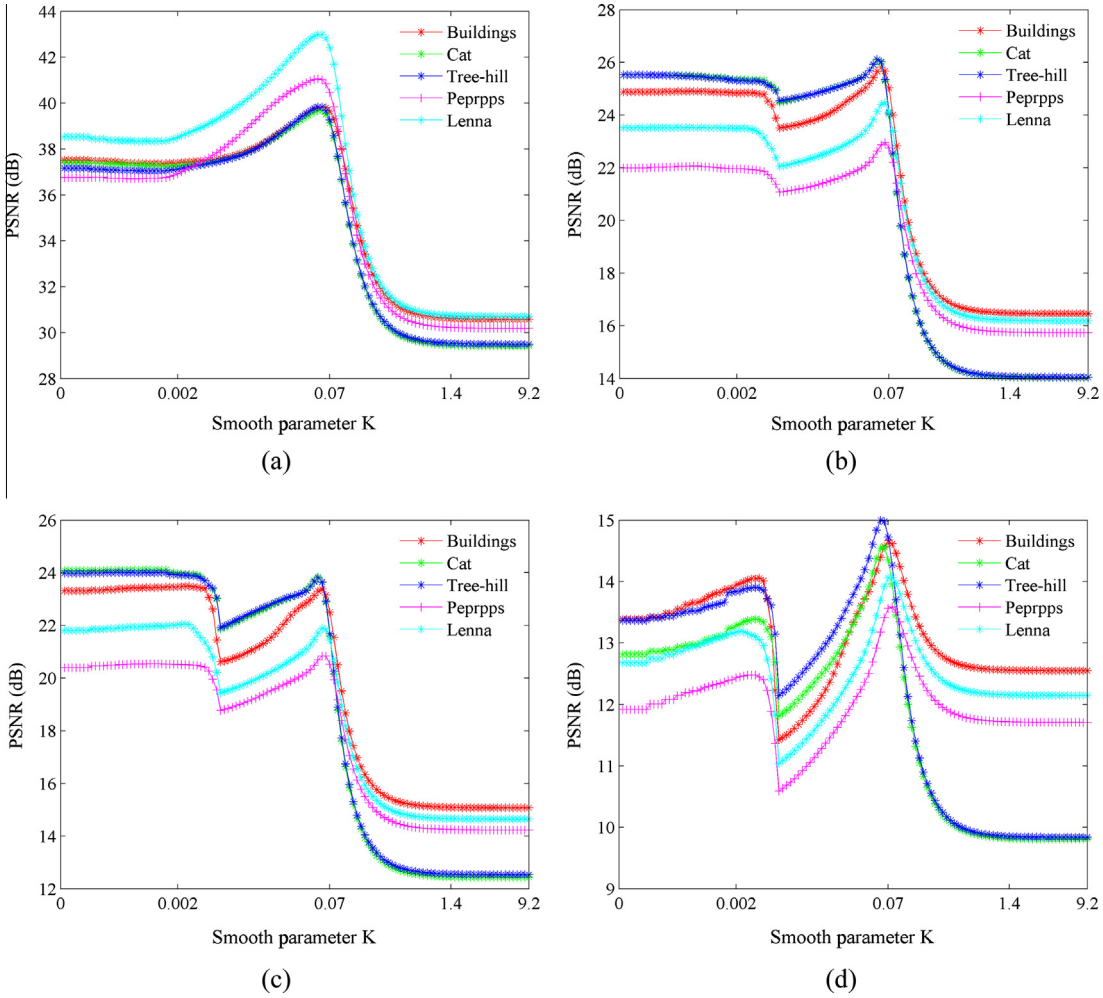

Fig. 4. The relation between K and the PSNR at certain noise level. (a) σ = 10%. (b) σ = 60%. (c) σ = 70%. (d) σ = 90%.

Table 1
The optimal values of K at every peak for different images with various noise density.

Images	Optimal values of K								
	10%	20%	30%	40%	50%	60%	70%	80%	90%
Building	0.0653	0.0718	0.0790	0.0790	0.0790	0.0956	0.0956	0.0956	0.1399
Cat	0.0593	0.0653	0.0718	0.0790	0.0790	0.0869	0.0956	0.0956	0.1156
Tree-hill	0.0593	0.0653	0.0718	0.0790	0.0790	0.0869	0.0956	0.0956	0.1156
Pepper	0.0593	0.0653	0.0718	0.0790	0.0869	0.1051	0.1051	0.1051	0.1399
Lena	0.0653	0.0718	0.0718	0.0790	0.0869	0.1051	0.1051	0.1051	0.1399

abruptly. Accordingly, noisy point will has a much higher indeterminacy in comparison with points in boundary areas.

Taking the Babala image as an example, we observe the valuable properties of neutrosophic indeterminacy. With a 3×3 filtering widow, the original and contaminated images are transformed into NS domain by using Eqs. (3–7), and their indeterminacy images are shown in Fig. 1. In weak texture or edge area such as the ellipse region in Fig. 1(b), pixels' uncertainty are slightly stronger, while in flat region such as the rectangle area, they are decreased even down to zero. However, as shown in Fig. 1 (c) and (d), the indeterminacy of noisy pixels in images corrupted with 1% and 10% noise density has been significantly enhanced.

Consequently, from above-descriptions, a conclusion can be drawn that indeterminacy information has the capability to distinguish the type of the area that the current pixel locates in.

3. Adaptive neutrosophic weight function

The powerful Gaussian kernel function described by Eq. (10) has been widely exploited in spatial filtering [25]. In the proposed filter, the weight of every pixel in the filtering window is modeled by this function, too.

$$F(x) = \exp\left(-\frac{x^2}{2h^2}\right). \tag{10}$$

In Eq. (10), h controls the degree of decay and affects the denoising performances, and it is related not only to the density of noise but also to the contents of images. The bigger the value of the parameter is, the smoother the restored image is, and vice versa. In [31], B. Smolka has proposed that image structure can be used to acquire the optimal h. Since neutrosophic indeterminacy can

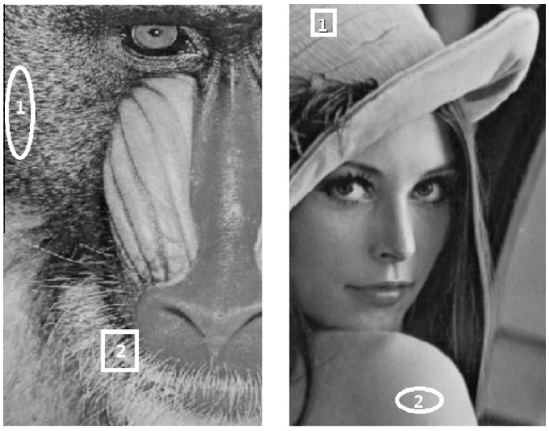

Fig. 5. Local zones in tested images. (a) Baboon. (b) Lena.

accurately discern the property of areas, it can be exploited to design the function for an adaptive h, and this will be discussed in Section 3.2.

The basic idea of image filtering is to update the detected noise by using its neighborhood information, and the restored value of the current pixel can be estimated as

$$g(x)' = \frac{\sum_{y\in D(x)} w(y) \times g(y)}{\sum_{y\in D(x)} w(y)}. \quad (11)$$

where $g(x)'$ is the denoising result of $g(x)$, $w(y)$ denotes the weight of the pixel at the location y, and $D(x)$ is the filtering window centered at x.

3.1. Similarity measurement

The weight function $w(\cdot)$ is determined by the similarity of pixels in $D(x)$ and plays a crucial role in noise removal. The fundamental difference of various filters is the strategy of designing weight function, in which a suitable and efficient feature used to measure pixel similarity is pretty critical. Spatial distance has been used in Gaussian filters and intensity distance has been taken into account in Yaroslavsky neighborhood filter [22]. While Bilateral Filter considers both Euclidean distance and gray-level of the neighboring pixels without smoothing edges [23]. In addition, gradient information has been adopted in [24]. In this paper, the feature of neutrosophic indeterminacy is innovatively regarded as a criterion of measuring similarity. Just as mentioned above, if a pixel has a lower indeterminacy, it signifies the current pixel has a reasonably higher similarity and closer correlation with surrounding pixels. Therefore, it should be allocated a larger weight in denoising. By contrast, if the uncertainty value is much stronger, this implies the current pixel has a much lower homogeneity and similarity

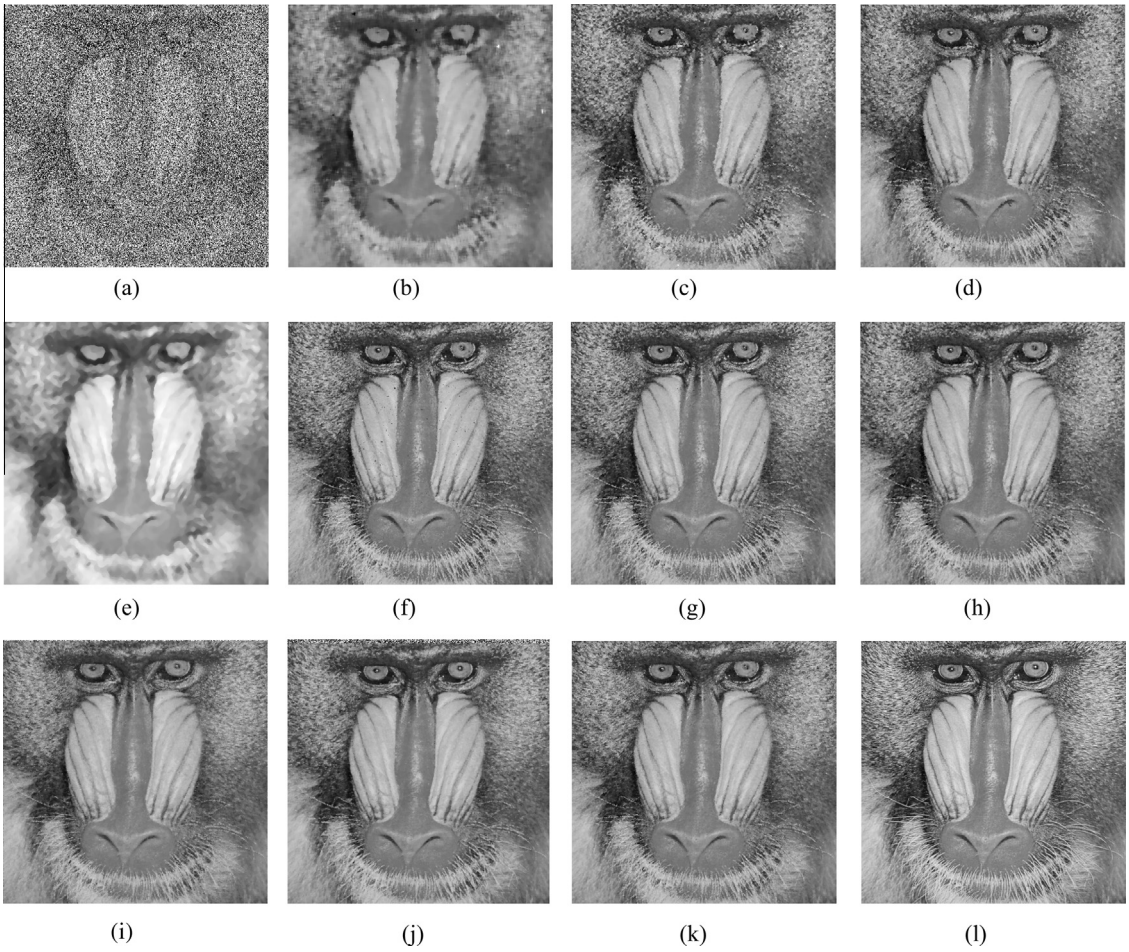

Fig. 6. Results of different filters for Baboon image. (a) Noisy image with 60% Salt and Pepper noise. (b) MF. (c) AMF. (d) DBA. (e) NEF. (f) MDBUTM. (g) FBDA. (h) DBTMF. (i) AICF. (j) TSF. (k) ANWF. (l) Original image.

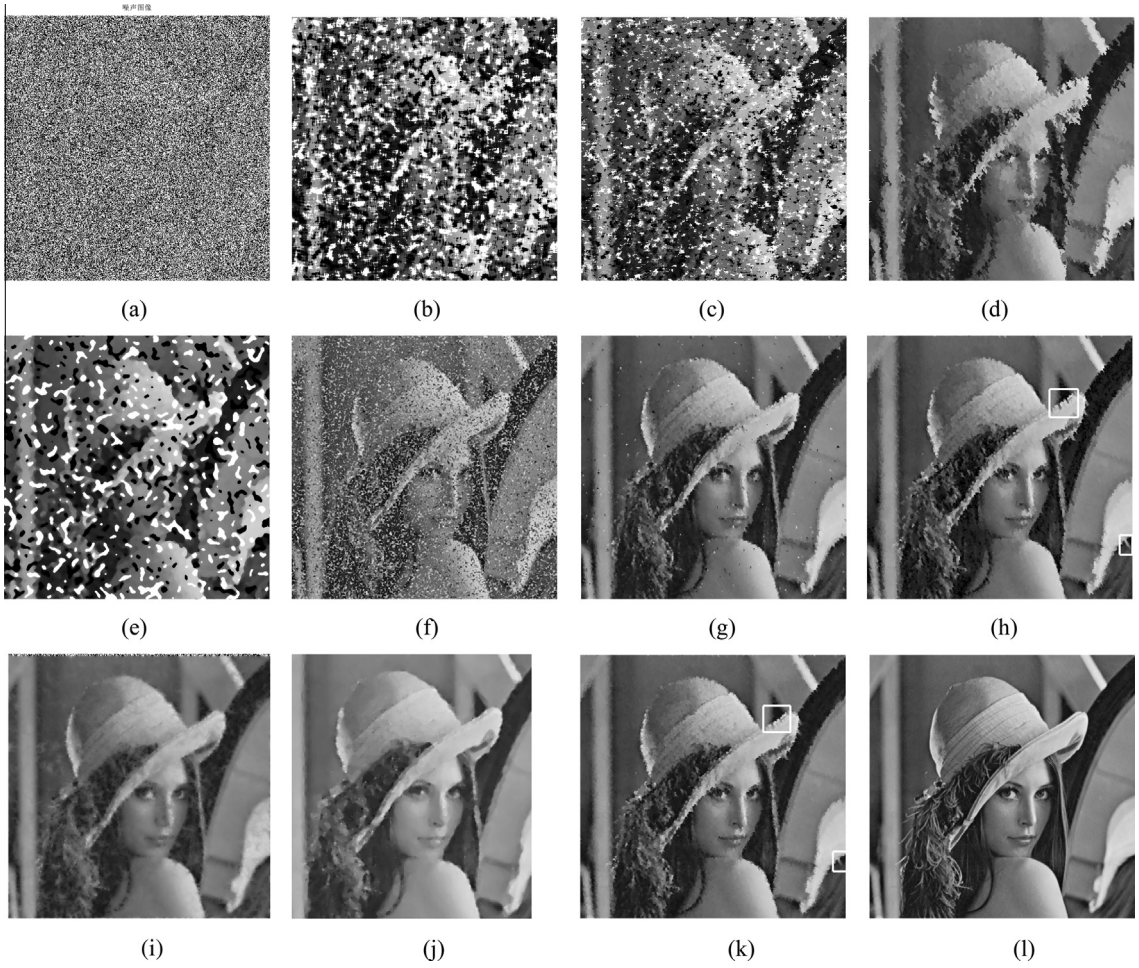

Fig. 7. Results of different filters for Lena image. (a) Noisy image with 90% Salt and Pepper noise. (b) MF. (c) AMF. (d) DBA. (e) NEF. (f) MDBUTM. (g) FBDA. (h) DBTMF. (i) AICF. (j) TSF. (k) ANWF. (l) Original image.

with neighboring pixels, so it should be distributed a weaker weight. In conclusion, indeterminacy can be selected as a robust characteristic of measuring similarity.

Modeled by Gaussian kernel function, an adaptive neutrosophic weight function based on indeterminacy can be considered as below,

$$w(y) = \frac{1}{C1}\exp\left(\frac{-I(y)^2}{2h^2}\right), \tag{12}$$

$$C_1 = \sum_{y\in D_{(x)}} \exp\left(\frac{-I(y)^2}{2h^2}\right). \tag{13}$$

where $I(y)$ is the indeterminacy of the pixel locating at y and calculated by Eqs. (3)–(5). h is the smoothing parameter of Gaussian kernel function and determines the approximate threshold above which to penalize high indeterminacy value. C_1 is the normalization constant described as Eq. (13). Since $I(y)$ varies from point to point, the value of $w(y)$ can be adaptively regulated with the variation of pixel's indeterminacy.

3.2. Pixel-wise adaptive smoothing parameter

In most denoising methods, h is selected by trial and error and kept constant in the whole image. For example, in [14], Buades et al. suggested $h = K * \beta$ for Gaussian noise reduction, where β is the standard deviation and the recommended value of K is between 10 and l5. In [7,16,26,27], methods of adaptive h have been studied deeply, but its value is maintained the same for all pixels in the whole image. However, in different parts of the image, it is rather difficult to find a globally fixed optimal parameter that can simultaneously ensure perfect denoising result and effective protection of details [28].

In detailed area, a smaller h is conducive to preserve the edges and textures, while in a flat region, a larger one can make all neighboring pixels almost have the equal weight and can enhance the smoothness of the restored area. That is to say, the value of h should be modified in different type of regions. Since pixel's indeterminacy has the faulty to distinguish the type of a region, it can be used to adjust the value of h, so a pixel-wise adaptive decay function on base of indeterminacy can be expressed as

$$h(y) = \exp(-2I(y)/I_{\max})/K. \tag{14}$$

where $h(y)$ is the smoothing parameter of the pixel locating at y, and $I(y)$ is the pixel's indeterminacy. $I_{\max}$ is the maximum in uncertain map of the corrupted image, and the coefficient 2 before $I(y)$ is used to reinforce the role of indeterminacy on $h(y)$.

Combining formulas (12–14), the weight of every pixel in the filtering window can be obtained as

$$w(y) = \frac{1}{C_2}\exp\left(-I(y)^2/2(\exp\left(-2I(y)/I_{\max}\right)/K)^2\right), \tag{15}$$

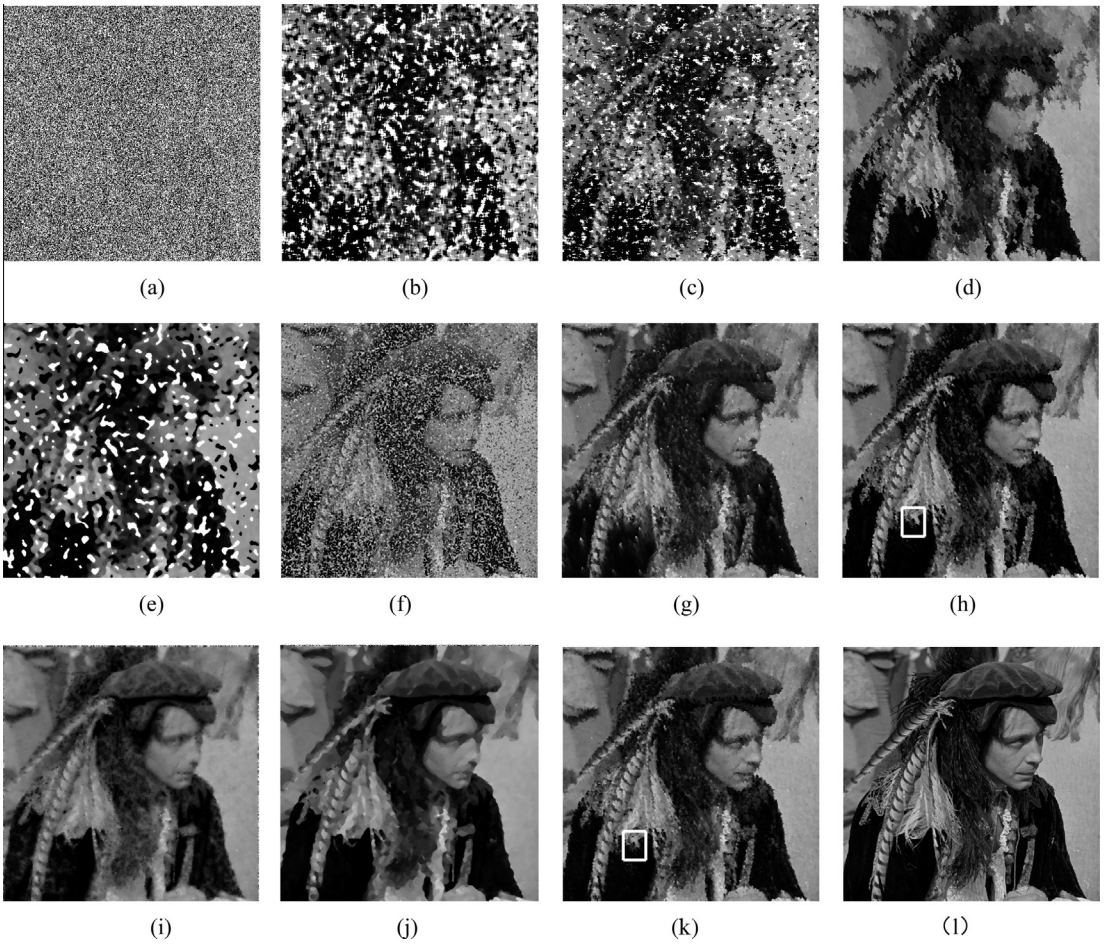

Fig. 8. Results of different filters for Man image. (a) Noisy image with 90% Salt and Pepper noise. (b) MF. (c) AMF. (d) DBA. (e) NEF. (f) MDBUTM. (g) FBDA. (h) DBTMF. (i) AICF. (j) TSF. (k) ANWF. (l) Original image.

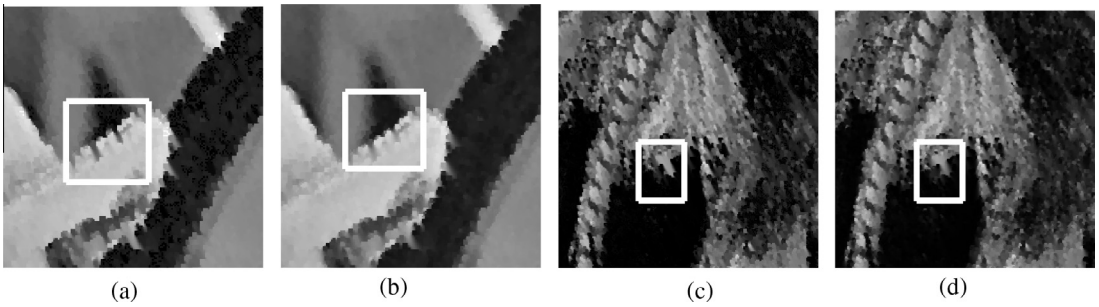

Fig. 9. Partial enlarged details of DBTMF and ANWF. (a) Partial enlarged detail of Lena image with DBTMF. (b) Partial enlarged detail of Lena image with ANWF. (c) Partial enlarged detail of Man image with DBTMF. (d) Partial enlarged detail of Man image with ANWF.

$$C_2 = \sum_{y \in D(x)} \exp\left(-I(y)^2 / 2(\exp(-2I(y)/I_{\max})/K)^2\right). \tag{16}$$

As an automatic way of adjusting $h(y)$ pixel by pixel, our object is to let K play the dominant role while $I(y)$ acts as an auxiliary factor. In other words, K keeps constant while $h(y)$ varies in accordance with $I(y)$. To achieve this objective, it is necessary to research the laws between the optimal K and a perfect denoising performance. The performance criterions applied in this paper are PSNR (Peak Signal to Noise Ratio) and MAE (Mean Absolute Error) defined by

$$PSNR = 10 \log \frac{255^2}{MSE}, \tag{17}$$

$$MAE = \frac{\sum_{i=0}^{M-1} \sum_{j=0}^{N-1} |Y(i,j) - Z(i,j)|}{MN}, \tag{18}$$

where MSE is expressed as

$$MSE = \frac{\sum_{i=0}^{M-1} \sum_{j=0}^{N-1} (Y(i,j) - Z(i,j))^2}{MN}. \tag{19}$$

Table 2
Comparisons of different filters for Baboon image at different noise levels.

Noise density (%)	Criterion	PSNR and MAE of different filters for restored images (Baboon)									
		MF [1]	AMF [4]	DBA [7]	NEF [17]	MDBU TMF [9]	FBDA [10]	DBTMF [11]	AICF [13]	TSF [12]	ANWF Ours
10	PSNR	23.06	23.09	31.64	25.41	32.15	26.57	24.81	32.35	32.78	**31.69**
	MAE	10.73	10.23	1.39	8.33	1.31	3.85	4.95	1.36	1.35	**1.38**
20	PSNR	21.05	22.32	28.12	24.85	28.79	26.05	24.31	29.06	29.95	**28.35**
	MAE	14.83	11.38	2.93	9.01	2.71	4.49	5.92	2.83	2.51	**2.85**
30	PSNR	20.80	21.50	25.93	24.02	26.75	25.38	23.72	27.29	27.87	**26.46**
	MAE	15.21	12.72	4.62	10.59	4.21	5.38	7.05	4.27	3.85	**4.34**
40	PSNR	20.27	20.81	24.32	24.88	25.30	24.61	23.21	24.83	25.09	**25.10**
	MAE	16.71	14.04	6.47	9.90	5.75	6.50	8.17	6.92	6.78	**5.85**
50	PSNR	19.94	20.16	22.81	24.11	23.82	23.65	22.58	22.94	23.87	**23.84**
	MAE	17.29	15.38	8.63	10.33	7.55	7.93	9.46	9.84	8.50	**7.59**
60	PSNR	19.57	19.49	21.44	23.18	22.49	22.69	21.96	22.10	22.30	**22.94**
	MAE	18.31	16.89	11.11	11.36	9.65	9.63	10.87	11.39	10.27	**9.04**
70	PSNR	18.65	18.60	20.05	21.34	20.77	21.20	21.17	21.10	21.64	**21.90**
	MAE	19.96	18.86	14.14	13.89	12.65	11.18	12.62	13.69	12.72	**11.44**
80	PSNR	14.79	16.09	18.77	15.77	18.44	20.28	20.24	19.42	20.04	**20.43**
	MAE	28.70	24.15	17.88	33.77	17.84	14.65	14.90	19.18	15.34	**14.32**
90	PSNR	9.47	11.28	17.15	8.44	15.67	19.11	18.91	18.62	19.32	**19.53**
	MAE	61.55	45.15	23.24	74.58	27.84	18.02	18.48	22.50	17.93	**17.24**

Table 3
Comparisons of different filters for Lena image at different noise levels.

Noise density (%)	Criterion	PSNR and MAE of different filters for restored images (Lena)									
		MF [1]	AMF [4]	DBA [7]	NEF [17]	MDBU TMF [9]	FBDA [10]	DBTMF [11]	AICF [13]	TSF [12]	ANWF Ours
10	PSNR	34.47	35.02	42.23	32.84	43.83	37.51	39.95	42.04	43.91	**43.23**
	MAE	2.20	1.88	0.34	3.42	0.29	0.89	0.41	0.38	0.18	**0.31**
20	PSNR	30.63	32.80	37.97	31.92	39.87	36.20	36.97	39.06	40.21	**38.98**
	MAE	3.92	2.49	0.76	3.73	0.63	1.15	0.83	0.68	0.41	**0.67**
30	PSNR	29.76	31.01	35.06	30.47	37.37	35.29	34.80	36.89	37.32	**36.97**
	MAE	4.28	3.16	1.28	4.83	1.02	1.40	1.33	1.16	0.86	**1.03**
40	PSNR	27.79	29.44	32.32	28.38	34.95	34.15	33.11	34.02	34.89	**34.75**
	MAE	5.44	3.91	1.96	6.61	1.52	1.77	1.89	1.91	1.22	**1.51**
50	PSNR	26.87	28.28	30.42	27.90	32.34	33.02	31.75	32.24	32.86	**33.36**
	MAE	5.90	4.62	2.72	6.50	2.09	2.17	2.47	2.70	1.79	**1.97**
60	PSNR	25.48	26.94	28.13	26.22	28.65	31.02	30.50	30.98	31.24	**31.66**
	MAE	7.04	5.44	3.79	7.32	3.06	3.12	3.13	3.39	2.41	**2.58**
70	PSNR	22.53	23.81	25.57	24.32	24.04	29.93	28.92	28.53	29.21	**29.97**
	MAE	8.84	7.02	5.04	8.79	5.43	3.48	4.03	4.97	3.26	**3.41**
80	PSNR	15.82	18.29	23.12	19.35	19.36	27.75	27.13	26.43	27.40	**28.19**
	MAE	17.79	12.08	7.08	17.79	11.21	4.61	5.23	6.91	4.73	**4.50**
90	PSNR	9.42	11.52	19.58	11.38	15.06	24.52	24.12	23.89	24.96	**25.43**
	MAE	53.79	35.32	13.07	41.74	25.34	7.05	7.74	11.08	6.93	**6.64**

where Y denotes the original image with a resolution of $M \times N$ and Z is the reconstructed one.

Tested images used in this paper are listed in Fig. 2. Taking Lena and Cat images as examples, Fig. 3 indicates the relation between K and PSNR performance at various noise level (σ = 10–80%). It is can be noted that When K <= 0.002, PSNR values are almost stable, and around K = 0.07, a distinct peak of PSNR appears. But with the increasing of K, PSNR values descent sharply. When the value of K is near to 1.4, the results remain stable again. When σ >= 60%, two peaks appear in these curves. The first peak is around K = 0.002 and the other is near to 0.07, but the corresponding PSNR of the second peak is much higher than that of the first one.

To further verify the persuasiveness and universality of above conclusions, extensive experiments on a large number of images have been implemented repeatedly. Fig. 4(a)–(d) are the typical results of the contaminated images with the noise density of 10%, 60%, 70% and 90%, respectively. From these results, it is can be seen that the law between PSNR and K almost remains the same as the rule shown in Fig. 3. To diverse images, the optimum values of K under various noise level are shown in Table 1.

As can be seen from Table 1, to a same image with a varying noise density from 10% to 90%, the values of K are not precisely the same. Likewise, to diverse images with the same noise density, the values of K are not fully identical, either. In a sense, these data

Table 4
Comparisons of different filters for Man image at different noise levels.

Noise density (%)	Criterion	PSNR and MAE of different filters for restored images (Man)									
		MF [1]	AMF [4]	DBA [7]	NEF [17]	MDBU TMF [9]	FBDA [10]	DBTMF [11]	AICF [13]	TSF [12]	ANWF Ours
10	PSNR	28.77	29.28	36.69	26.65	36.17	31.20	31.77	37.06	38.12	**36.23**
	MAE	4.84	4.37	0.73	8.69	0.80	2.10	1.32	0.71	0.64	**0.84**
20	PSNR	25.78	27.83	33.24	23.60	32.90	30.22	30.45	34.03	34.53	**33.03**
	MAE	7.29	5.19	1.48	8.34	1.53	2.58	2.08	1.43	1.39	**1.56**
30	PSNR	25.32	26.51	30.66	25.76	30.27	29.29	29.28	29.31	32.45	**31.25**
	MAE	7.65	6.08	2.36	9.09	2.40	3.17	2.86	3.39	2.06	**2.22**
40	PSNR	23.85	25.28	28.46	25.74	28.07	28.23	28.12	28.91	30.86	**29.47**
	MAE	9.28	7.11	3.46	7.83	3.42	3.94	3.79	3.91	2.82	**3.15**
50	PSNR	23.32	24.27	26.59	25.09	25.92	27.05	27.15	27.62	29.32	**28.15**
	MAE	9.80	8.12	4.75	8.05	4.67	4.86	4.72	5.06	3.66	**4.04**
60	PSNR	22.27	23.12	24.84	24.03	23.21	26.02	26.20	26.00	27.08	**26.89**
	MAE	11.22	9.33	6.37	7.90	6.59	5.90	5.76	6.78	5.28	**5.09**
70	PSNR	20.38	21.31	22.87	22.00	20.05	24.90	25.07	24.59	25.49	**25.70**
	MAE	12.99	11.05	8.56	11.53	10.16	7.25	7.08	8.65	6.70	**6.32**
80	PSNR	14.99	16.90	20.68	17.71	16.53	23.22	23.52	23.02	23.59	**24.07**
	MAE	21.83	16.47	11.90	21.55	17.71	9.26	8.85	11.15	9.10	**8.12**
90	PSNR	8.82	10.61	17.89	10.40	12.84	20.84	21.17	20.88	21.90	**22.04**
	MAE	56.73	39.88	18.26	46.40	34.88	13.28	12.30	15.43	11.14	**11.22**

can explain the reason why a globally constant smoothing parameter is inadvisable. In addition, it is clear that when $\sigma >= 60\%$, the values of K are relatively larger than those of $\sigma < 60\%$. In order to simplify the assigning of K, when $\sigma < 60\%$, as the median of all values, 0.0718 is selected as the most optimal value of K, and 0.0956 is regarded as the optimum in other cases. On the whole, the constant K can be assigned as follows

$$\begin{cases} K = 0.0718, & \sigma < 60\% \\ K = 0.0956, & others \end{cases} \tag{20}$$

After replacing K with 0.0718 or 0.0956 in Eq. (14), the value of $h(y)$ will be different from point to point on account of a pixel-wise $I(y)$. For example, in Fig. 5, Baboon and Lena are contaminated by the noise with density of 90%, and two local zones in these two images are selected, respectively. In a 3×3 filleting window, the smoothing parameter matrixes h_{B1} and h_{B2} of Baboon and h_{L1} and h_{L2} of Lena are indicated below.

$$h_{B1} = \begin{bmatrix} 40.3627 & 1.8849 & 4.0974 \\ 13.9276 & 13.9276 & 13.9276 \\ 3.1879 & 13.9276 & 8.2349 \end{bmatrix}$$

$$h_{B2} = \begin{bmatrix} 12.9783 & 13.3920 & 5.3495 \\ 6.1125 & 5.9704 & 10.5842 \\ 5.3495 & 5.2251 & 5.1438 \end{bmatrix}$$

$$h_{L1} = \begin{bmatrix} 1.8849 & 1.8849 & 1.8849 \\ 3.7587 & 3.5025 & 13.9726 \\ 3.7587 & 13.9276 & 13.9726 \end{bmatrix}$$

$$h_{L2} = \begin{bmatrix} 5.3077 & 13.8188 & 5.0242 \\ 5.3916 & 4.9460 & 5.2663 \\ 1.8849 & 5.4341 & 4.9460 \end{bmatrix}$$

It is obvious that in h_{B1}, h_{B2}, h_{L1} and h_{L2}, the value of every pixel's smoothing parameter is adaptively regulated from point to point. So far, the object that the decay parameter can be pixel-wise adjusted according to the specific contents of images has been achieved.

4. Experimental results

In ANWF, if a pixel has a gray value of 0 or 255 in 8-bit images, it is labeled as noise candidate and its location is recorded in the noise matrix *BNM*. To a noisy pixel, the corresponding value in *BNM* is 0, otherwise, it is 1. In Eq. (20), σ is used to determine the value of K, but from Figs. 3 and 4 and Table 1, it is can be deduced that in a certain smaller range, noise density has small impact on K. Accordingly, a rough estimation of σ can meet our requirements. Hence it can be roughly estimated as follows

$$\sigma = \frac{\text{number of } 0'\text{s in } BNM}{\text{total number of pixels in the image}}. \tag{21}$$

In filtering stage, noise candidates are disposed while noise-free points are kept intact. What is more, only the uncontaminated pixels are exploited to replace the corrupted one.

The proposed ANWF is compared with some state-of-the-art methods, such as MF [1], AMF [4], DBA [7], NEF [17], MDBUTMF [9], FDBA [10], DBTMF [11], TSF [12] and AICF [13]. In order to compare fairly, MF, NEF, AMF and TSF are operated with their most suitable window sizes changing from 3×3 to 9×9, while ANWF and the left algorithms are implemented with a fixed 3×3 window. Extensive experiments have been performed on various images corrupted by SPN with varying noise density from 10% to 90% with increment of 10%. All experiments are executed in MATLAB R2013a and run on a PC with Intel Core i7-4700MQ 2.4 GHz CPU.

4.1. Visual quality evaluation

Visual comparisons of the recovered images such as Lena, Baboon and Man are shown in Figs. 6–9, respectively. In Fig. 6, when $\sigma = 60\%$, all filters can eliminate noise efficiently, but image details are blurred slightly by MF and NEF. Moreover, it may be the iterative operation of γ-median that makes the blurring of image is much heavier in Fig. 6(e) than in Fig. 6(b). When noise level soars to 90%, the performances of MF, AMF, NEF, DBA and MDBUTMF are all influenced badly, and as shown in Figs. 7 and 8, noise blocks increase considerably in their restored images. In the images recovered by FBDA, noisy points have not been eliminate completely and a lot of stains are still remained. In addition,

images restored by ACIF look fairly hazy. The visual qualities of DBTMF and TSF are as excellent as ANWF; however, as it seen from the partially enlarged details in Fig. 9(a)–(d), the jagged edges of DBTMF are more evident than that of ANWF. Although edges are preserved satisfactorily by TSF, unfortunately, the over-smoothing phenomenon is pretty apparent, which leads to a bad visual effect. For example, the textures of Lena hat and the man's hair cannot be clearly identified in Figs. 7(j) and 8(j). In a word, ANWF performs significantly better than many other existing techniques in term of visual quality.

4.2. Quantitative evaluation

To further demonstrate the effectiveness of ANWF, the comparative results of PSNR and MAE of the ten methods are shown in Tables 2–4. When noise level is less than 40%, the most competitive PSNR and MAE performances are produced by TSF. In Table 2, when noise level approximately rise to 50–60%, the PSNR value of NEF excels ANWF, but from Fig. 6(e) and (j), it is can be detected that ANWF has more prominent visual effect than the former. Especially when noise level amounts to 70–90%, the proposed algorithm shows its superior performances in PSNR and MAE.

5. Conclusion

In this paper, an adaptive neutrosophic filter based on pixel's indeterminate information has been presented to remove high-density SPN. In order to accurately measure pixel similarity, a novel and effective criterion based on Neutrosophic indeterminacy is utilized in the weight function. Meanwhile, for the purpose of adjusting the smooth parameter according to the contents of image, the Neutrosophic indeterminacy is exploited to distinguish the area type to which a pixel belongs, and as a regulatory factor, it controls the variation of smoothing parameter in cooperation with a constant K. With a fixed 3×3 window, the proposed method can obtain remarkable performances in terms of visual quality and quantitative evaluation especially for high-level SPN.

Acknowledgments

This work was supported by the National Natural Science Foundation of China (Grant No. 61203330), the Department of Science and Technology of Shandong Province (Grant No. 2015ZDXX0801A01) and the Fundamental Research Funds of Shandong University (Grant No. 2015QY001).

References

[1] J.W. Tukey, Nonlinear methods for smoothing data, in: Proceedings of Electronics and Aerospace Systems Conference, 1974, pp. 673–681.
[2] M. Nasri, S. Saryazdi, H. Nezamabadi-pour, SNLM: a switching non-local means filter for removal of high density salt and pepper noise, Scientia Iranica 20 (2013) 760–764.
[3] K.S. Srinivasan, D. Ebenezer, A new fast and efficient decision-based algorithm for removal of high-density impulse noises, IEEE Signal Process. Lett. 14 (2007) 189–192.
[4] R.H. Chan, C.W. Ho, M. Nikolova, Salt-and-pepper noise removal by median-type noise detectors and detail-preserving regularization, IEEE Trans. Image Process. 14 (10) (2005) 1479–1485.
[5] H. Ibrahim, N.S.P. Kong, T.F. Ng, Simple adaptive median filter for the removal of impulse noise from highly corrupted images, IEEE Trans. Consum. Electron. 54 (2008) 1920–1927.
[6] S.J. Horng, L.Y. Hsu, T. Li, Using sorted switching median filter to remove high-density impulse noises, J. Vis. Commun. Image Represent. 24 (2013) 956–967.
[7] K.S. Srinivasan, D. Ebenezer, A new fast and efficient decision-based algorithm for removal of high-density impulse noises, IEEE Signal Process. Lett. 14 (3) (2007) 189–193.
[8] X. Zhang, Y. Xiong, Impulse noise removal using directional difference based noise detector and adaptive weighted mean filter, IEEE Signal Process. Lett. 16 (4) (2009) 295–298.
[9] S. Esakkirajan, T. Veerakumar, Adabala N. Subramanyam, et al., Removal of high density salt and pepper noise through modified decision based unsymmetric trimmed median filter, IEEE Signal Process. Lett. 18 (5) (2011) 287–290.
[10] Madhu S. Nair, G. Raju, A new fuzzy-based decision algorithm for high-density impulse noise removal, Signal Image Video Process. 6 (2012) 579–595.
[11] V.R. Vijaykumar, G. Santhanamari, New decision-based trimmed median filter for high-density salt-and-pepper noise removal in images, J. Electron. Imag. 23 (3) (2014) 033011–033014.
[12] G. Gao, Y. Liu, An efficient three-stage approach for removing salt and pepper noise from digital images, Int. J. Light Electron Opt. 126 (2015) 467–471.
[13] X.Q. Zhang, F. Ding, Z.H.J. Tang, Salt and pepper noise removal with image inpainting, Int. J. Electron. Commun. 69 (2015) 307–313.
[14] A. Buades, B. Coll, J.M. Morel, A review of image denoising algorithms, with a new one, Multiscale Model. Simul. 4 (2005) 490–530.
[15] D. Van De Ville, M. Kocher, SURE-based non-local means, IEEE Signal Process. Lett. 16 (2009) 973–976.
[16] T. Tasdizen, Principal neighborhood dictionaries for nonlocal means image denoising, IEEE Trans. Image Process. 18 (2009) 2649–2660.
[17] Y.H. Guo, H.D. Cheng, Y. Zhang, A new neutrosophic approach to image denoising, New Math. Natural Comput. 5 (2009) 653–662.
[18] M. Zhang, L. Zhang, H.D. Cheng, A Neutrosophic approach to image segmentation based on watershed method, Signal Process. 90 (2010) 1510–1517.
[19] Y.H. Guo, H.D. Cheng, New Neutrosophic approach to image segmentation, Pattern Recogn. 42 (2009) 587–595.
[20] P.A. Loeb, M. Wolff, Nonstandard Analysis for the Working Mathematician, Kluwer, Dordrecht, Netherlands, 2000.
[21] Y.H. Guo, A. Sengur, A novel color image segmentation approach based on neutrosophic set and modified fuzzy c-means, Circ. Syst. Signal Process. 32 (2013) 1699–1723.
[22] B. Zhang, J.P. Allebach, Adaptive bilateral filter for sharpness enhancement and noise removal, IEEE Trans. Image Process. 17 (2008) 664–678.
[23] A. Senjian, B. Farid, B. Mohammed, S. Ferdous, Quantitative error analysis of bilateral filtering, IEEE Signal Process. Lett. 22 (2015) 202–206.
[24] P. Perona, Malik, Scale-space and edge detection using anisotropic diffusion, IEEE Trans. Pattern Anal. Mach. Intell. 12 (1990) 629–639.
[25] J. Portilla, V. Strela, M.J. Wainwright, E.P. Simoncelli, Image denoising using scale mixtures of Gaussians in the wavelet domain, IEEE Trans. Image Process. 12 (2003) 1338–1351.
[26] G. Xu, J. Tan, A universal impulse noise filter with an impulse detector and nonlocal means, Circ. Syst. Signal Process. 33 (2014) 421–435.
[27] M. Nasri, S. Saryazdi, H. Nezamabadi-pour, A fast adaptive salt and pepper noise reduction method in images, Circ. Syst. Signal Process. 32 (2013) 1839–1857.
[28] T. Brox, D. Cremers, Iterated nonlocal means for texture restoration, in: Proceedings of the 1st International Conference on Scale Space and Variational Methods in Computer Vision, vol. 4485, 2007, pp. 13–24.
[29] A.Q. Ansari, Ranjit Biswasb, Swati Aggarwalc, Neutrosophic classifier: an extension of fuzzy classifier, Appl. Soft Comput. 13 (2013) 563–573.
[30] Abdulkadir Sengur, Yanhui Guo, Color texture image segmentation based on neutrosophic set and wavelet transformation, Comput. Vis. Image Understand. 115 (2011) 1134–1144.
[31] B. Smolka, R. Lukac, A. Chydzinski, Fast adaptive similarity based impulsive noise reduction filter, Real-Time Imag. 9 (2003) 261–276.